Available online at www.sciencedirect.com
ScienceDirect
Polymer 47 (2006) 7339–7348
polymer
www.elsevier.com/locate/polymer

Structure and thermal properties of multilayered Laponite/PEO nanocomposite films

Eduard A. Stefanescu [a], Patrick J. Schexnailder [a], Avinash Dundigalla [a], Ioan I. Negulescu [a], Gudrun Schmidt [a,b,*]

[a] Department of Chemistry, Louisiana State University, Baton Rouge, LA 70803, USA
[b] Department of Biomedical Engineering, Purdue University, 206 S. Intramural Drive, West Lafayette, IN 47907-2032, USA

Received 5 June 2006; received in revised form 16 August 2006; accepted 17 August 2006
Available online 11 September 2006

Abstract

The structures and thermal properties of a series of nanocomposite poly(ethylene oxide)/Laponite films have been investigated by differential calorimetric and thermal analysis and complemented by microscopy and X-ray diffraction experiments. The crystalline structures of the nanocomposite multilayered films can be tuned by controlling the composition, polymer Mw and the water content. We study the concentration, polymer Mw and humidity dependence of polymer crystallinity in selected nanocomposite multilayered films. Results show that the exact sample preparation and history are important in controlling structure and properties and in developing new materials. Complementary microscopy is used to monitor the structural changes.

Keywords: Laponite; Poly-ethylene-oxide (PEO); Nanocomposite

1. Introduction

Developing nanocomposite membranes and films made from specialized polymer electrolyte materials are a promising direction toward improved energy storage needs. The addition of inorganic nanoparticles to polymer electrolytes is used to improve electrochemical performance [1–6]. However, applications of conventional composites are still hindered by low ionic conductivity at room temperature and difficulties in processing [7]. Conductivity is influenced by the presence of randomly oriented polymer crystallites that impede ionic mobility [8]. The knowledge and control of crystallinity at the nanometer length scale are critical in tailoring polymer–nanoparticle interactions and thus desired properties. By inducing anisotropy over large length scales and via supramolecular order, ways are found for fabricating scientifically and technologically novel materials [9,10].

Supramolecular polymer–nanoparticle composites combine the advantages of tailored nanometer structures with self-assembly on all length scales. Design and fabrication of polymer–nanoparticle electrolytes from solutions and gels allow for solid polymer electrolytes to be shaped around nearly any form. In the absence of defects and impurities these materials are transparent [11] with highly regular d_{001} reflections in diffraction patterns [11–13]. Recent work has investigated such materials [11–18]. We have shown that in solution, synthetic clay nanoparticles are exfoliated and act as multifunctional cross-links to poly(ethylene oxide) (PEO) polymers, thereby building a network [17,18]. The shear-orientation of this network, combined with simultaneous solvent evaporation, allows for the spontaneous assembly of unique supramolecular multilayered films [11,19]. The resulting transparent films have highly ordered structures with sheet-like layers of oriented nanoparticles [11]. In these films, the polymer crystallization in confinement and under shear flow is not well understood

* Corresponding author. Purdue University, Department of Biomedical Engineering, 206 S. Intramural Drive, West Lafayette, IN 47907-2032, USA. Tel.: +1 765 496 1427; fax: +1 765 496 1912.
E-mail address: gudrun@purdue.edu (G. Schmidt).

0032-3861/$ - see front matter © 2006 Elsevier Ltd. All rights reserved.
doi:10.1016/j.polymer.2006.08.051

and is the subject of much speculation. Understanding the origin of these highly ordered structures requires a fundamental study.

The exfoliation, intercalation and aggregation of clays in PEO nanocomposites have been extensively studied in the past [1–3,7,12,20,21]. The dispersion of clay platelets in polymer nanocomposite films can be achieved using a variety of techniques [3,7,22]. Intercalation of PEO chains between the inorganic clay layers has been shown to reduce or completely suppress polymer crystallinity, depending on the polymer–clay composition as well as other parameters such as salt, humidity, structural defects, etc [1,2]. Cation movement in the clay interlayer space is radically improved by coordination to the polymer that easily replaces the water molecules of hydration [3]. Unfortunately the polymer crystallinity as well as ionic conductivity of the nanocomposites is often not reproducible and strongly depends on the thermal history of the samples as can be observed in different heating cycles of thermal experiments [23]. The amount of polymer adsorbed to the clay is controlled by the layer charge density on the clay [20]. For example, in PEO–Montmorillonite nanocomposites the heterogeneous nucleation of PEO competes with the PEO coordination to sodium ions, which inhibits PEO crystallinity [9,10,24]. Although it has been found that ionic transport in polymer electrolytes occurs in the amorphous PEO phases above their glass transition, ionic conductivity in the polymer crystalline phase has also been observed [9,10]. The amount and orientation of the crystalline phase are thus very important in controlling specific properties.

Commercially available PEO is usually crystallized from solution. A powdery sample of chain-folded crystals is obtained, which usually ensures a relatively high degree of polymer crystallinity. Differential Scanning Calorimetry (DSC) and Temperature-modulated DSC (TMDSC) are excellent methods for monitoring such crystallinity, especially the reversibility of polymer molecular motions at different polymer molecular weights (Mw) [25,26]. DSC and TMDSC measurements have shown that for PEO with $Mw > 200$ kg/mol, a reversing and reversible latent heat contributes greatly to the apparent heat capacity during melting and crystallization [27]. This reversing latent heat decreases with time before reaching reversibility. Shorter PEO chains, $Mw = 1–5$ kg/mol, are usually very well crystallized and show almost no reversible effects upon melting [25,26]. The addition of clay nanoplatelets to the polymer will certainly complicate the thermal and structural behaviors of a resulting nanocomposite. The driving force behind polymer adsorption to the clay is entropic and involves replacement of any hydrated water [12,13]. PEO competes with the water that is binding to the clay making the water–PEO–Laponite clay system even more difficult to understand [28,29]. The kinetics of water adsorption in polyelectrolytes has been previously studied to correlate the film confinement, the thickness of the film, or the number of layers in the film with the amount of adsorbed water and water mobility. Specular X-ray reflectivity measurements on single layer polyelectrolyte films show that the water adsorption is dependent on the film thickness, where the water diffusion coefficient can be regulated by controlling the film confinement [30]. For the dynamics of water adsorption in multilayered polyelectrolyte films, nuclear magnetic resonance studies revealed that the water mobility increases when the number of layers in the film is increased [31].

The objective of the present contribution is to study the humidity dependent thermal properties of selected multilayered nanocomposite films as a function of polymer Mw and composition. Differential Scanning Calorimetry (DSC) is used to monitor changes in polymer crystallinity in the films and Thermogravimetric Analysis (TGA) is used to investigate the amount of adsorbed water found in the samples before and after exposure to humidity. Complementary microscopy monitors the structural changes due to water adsorption.

2. Experimental

Laponite-RD (LRD), a synthetic Hectorite type clay (Southern Clay Products) was used as received without any further purification. The LRD clay platelets are 30 nm across and ca. 1 nm thick charged discs. Poly(ethylene-oxide) (PEO) with molecular masses of 100 kg/mol, 300 kg/mol, 600 kg/mol, and 1000 kg/mol were purchased from Polysciences Inc. Multilayered films were prepared via gel/solution exfoliation [17–19]. Optimal exfoliated solutions and gels can be obtained for a particular polymer–clay ratio, pH and ionic strength [14–16,32]. While ideally one would like to limit the number of parameters being altered in solution, this is often impossible due in large part to the very complicated phase diagrams of these complex polymer–clay systems [32,33]. Thus the choice of samples that are homogeneous and thermodynamically stable solutions especially at high concentrations is limited by their phase diagrams. Sample preparation of solutions and gels can be reduced to <3 weeks when samples are mixed/sheared and centrifuged daily [17,18]. Simply dissolving the polymer and the clay in water is not sufficient to completely exfoliate our samples: extensive mixing and shear are necessary to guarantee reproducibility of experiments [17,18]. All polymer–clay solutions and gels used to prepare films were exfoliated, homogeneous and stable (no degradation) for more than half a year [17,18,33,34].

The multilayered films are usually prepared by sequential adsorption of a thick layer of nanocomposite hydrogel or solution followed by slow solvent evaporation. While one spread and dried film already produces multilayers, we use sequential absorption to obtain thicker films simply for better investigation and handling [11,32–34]. Another major motivation to use a combined spreading and drying procedure for the nanocomposite films is the ability to obtain well-dispersed and oriented multilayers, which would otherwise be nearly impossible to prepare using conventional methods. Spincasting or dipping of the gum-like hydrogels and solutions was problematic due to their high viscosity and elasticity as well as impurities that were hard to remove. While one single spread film produces multilayers, conventional multilayer fabrication techniques such as layer-by-layer approaches or the Langmuir–Blodgett method would have to add each layer individually [11,19].

Depending on the concentration, transparent PEO–LRD single films with an average layer thickness of 5 μm–7 μm can be obtained by manually spreading the polymer–clay gel/solution on a glass substrate. Reproducible results are obtained when using and comparing two preparation techniques: (i) a simple spreading device can be used that guarantees the same thickness of each spread layer (but not the same shear rate) and (ii) the films are spread manually with a blade [19]. Manual spreading does not allow for shear rate controlled spreading either. For this work we have chosen only those solutions and gels for film preparation, where the shear rate and exact film thickness are not critical to the final film structure and where the multilayer size and order can be reproduced easily. All the other solutions and gels that have produced interesting supramolecular structures were not investigated here in detail because results could not be reproduced satisfactorily.

Specifically for this work, gels and solutions were manually spread onto glass slides layer-by-layer, the solvent was evaporated slowly and then the films were dried at 25 °C in desiccators and under vacuum. Following this procedure two distinct series of LRD–PEO multilayered films were produced: a first series comprised of samples containing PEO of 1000k Mw in different ratios with the LRD clay (LRD–PEO 60:40, 40:60, 15:85) (Table 1), and a second series of samples containing 60% Laponite clay and 40% PEO (w/w) of different molecular weights (100k, 300k, 600k, 1000k Mw) (Table 1). All the samples that were to be exposed to moisture at room temperature were placed under vacuum for 48 h; the vacuum was removed by the use of argon as an inert media. Films were then transferred to desiccators containing a beaker with water as a source of humidity. The desiccator was hermetically closed and the films were removed after precise periods of exposure to humidity (e.g. 3 h, 6 h, 12 h, etc).

Optical microscopy was performed using an Olympus BX51TF microscope with crossed polarizers. When sample preparation and history are kept the same, duplicate measurements on all instruments showed excellent reproducibility with a relative uncertainty of ca. 5%. Scanning Electron Microscopy (SEM) experiments were performed using a Cambridge 260 Stereoscan Electron Microscope. Only representative images are presented. The layered textures of the selected *x*–*y* SEM images of LRD60%–PEO40%–*X* were not uniform. LRD60%–PEO40%-1000 was calculated to have an average dimension of $d_{SEM} \approx 0.3 \pm 0.17$ μm per layer. More structural details of selected other samples were discussed in a previous study [11].

Table 1
Nanocomposite film composition and crystallinity as obtained from DSC measurements

Sample name	LRD conc. (%)	PEO Mw (kg/mol)	% Crystallinity (+/−5%)
LRD60%–PEO40%-*X*			
LRD60%–PEO40%-100	60	100	1.93
LRD60%–PEO40%-300	60	300	1.12
LRD60%–PEO40%-600	60	600	1.20
LRD60%–PEO40%-1000	60	1000	1.57
LRD-*Y*–PEO-*Z*-1000k			
LRD60%–PEO40%-1000	60	1000	1.57
LRD40%–PEO60%-1000	40	1000	78
LRD15%–PEO85%-1000	15	1000	94

X-ray diffraction measurements were done using a Siemens–Bruker D5000 X-ray Diffractometer with the Cu Kα radiation, of 1.54 Å. DSC experiments were performed using a TA 2920 MDSC instrument. Samples of 6.5–10 mg were subjected to analysis using a heating rate of 20 °C/min in two successive heating cycles. In all DSC traces, positive going features correspond to exothermic processes, and negative going features correspond to endothermic processes. For each measurement, a fresh nanocomposite sample was used in the first heating run followed by cooling and a second heating run. Thermogravimetric analyses (TGA) were performed in nitrogen atmosphere with a heating rate of 20 °C/min using a TA 2950 thermo balance. Only freshly prepared samples of ca. 7–11 mg were subjected to thermogravimetric analysis. TA Universal Analysis software was used for the integration and processing of all curves resulted from both instruments. Duplicate measurements on both instruments showed excellent reproducibility with a relative uncertainty of less than 5% when sample preparation and history were kept the same.

3. Results and discussion

3.1. Concentration dependence of structure and thermal properties

In a first series of experiments, we show the concentration dependence of DSC of representative nanocomposites with the same sample history (Fig. 1 and Table 1). Measurements are shown for LRD-*Y*–PEO-*Z*-1000 films containing 60%, 37.5% and 15% of LRD by weight. As expected, a large difference in the heat of fusion results in different crystallinities (Table 1) and

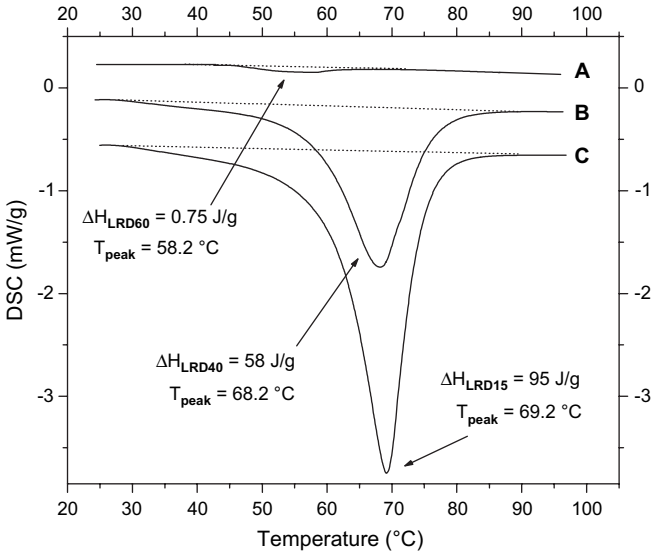

Fig. 1. Normalized DSC traces for the melting of nanocomposite films with different composition. (A) LRD60%–PEO40%-1000 kg/mol, (B) LRD40%–PEO60%-1000 kg/mol, and (C) LRD15%–PEO85%-1000 kg/mol.

the peaks observed in Fig. 1 shift to lower melting temperatures with increasing clay concentration. If we assume that any free excess polymer that is not attached to the clay is mostly crystalline then the crystallinity for LRD40%–PEO60%-1000 and LRD15%–PEO85%-1000 indicates that these two samples may contain very high amounts of excess polymer. The adsorbed and intercalated polymer is assumed to be mostly amorphous suggesting a maximum of 22% PEO and 6% PEO that may be adsorbed to the clay surfaces. Fig. 2 shows optical microscopy of the films discussed above as well as a reference pure polymer film. Complementary to the DSC results, the crystallinity increases with increased polymer concentration. In addition to the expected large spherulites that are observed for the reference pure PEO film (Fig. 2d) small ''dots'' are visible for the nanocomposites (Fig. 2b,c) suggesting differences in nucleation and growth of PEO crystals.

LRD60%–PEO40%-1000 films indicate very low crystallinity in DSC, which cannot be detected with polarized optical microscopy. This low crystallinity is due to the high clay content but is also influenced by the complete clay exfoliation and supramolecular structural orientation. The origin and specific structural details of LRD60%–PEO40% have been described elsewhere [11]. Most recently we have discovered that crystallinity changes after ca. one year, especially after repeated exposure of films to humidity and UV. These long-term studies, however, are not the subject of this work.

In Fig. 3 we investigate the composition dependent structure as obtained from SEM. Images in the $x-y$ plane (side surface fracture) show that the occurrence of micron size layers is strongly dependent on clay content. The definition of planes in Fig. 3d is also shown for better comparison, but the physical picture of general platelet orientation as obtained from our past study [11] corresponds only to LRD60%–PEO40%-1000. Although all samples were made from exfoliated polymer–clay solutions, LRD40%–PEO60%-1000 and LRD15%–PEO85%-1000 exhibited fewer or no layers, suggesting that the clay concentration is critical in layer production. X-ray diffraction (XRD) results are shown in Fig. 4. At high clay concentrations and dense packing, platelets have no other choice than to stack and order, producing many regular XRD reflections that correspond to the PEO intercalated and stacked clay. Such regular reflections have been observed in the past for other clay nanocomposites [7,19]. At higher polymer concentrations such as LRD40%–PEO60%-1000, XRD reflections still occur at the same q but their intensity is much weaker, suggesting the presence of fewer stacked clay domains in the polymer matrix. LRD15%–PEO85%-1000 shows no more regular reflections but instead peaks that can be correlated to reflections from the crystalline polymer (Fig. 4b). LRD15%–PEO85%-1000 has exfoliated clay platelets in the polymer matrix but the clay platelets are too far apart and too randomized to produce higher order reflections. Nevertheless on the nanometer length scale as detected by Small Angle Neutron Scattering (SANS) we have shown that on average even these clay platelets orient in the spread direction [32].

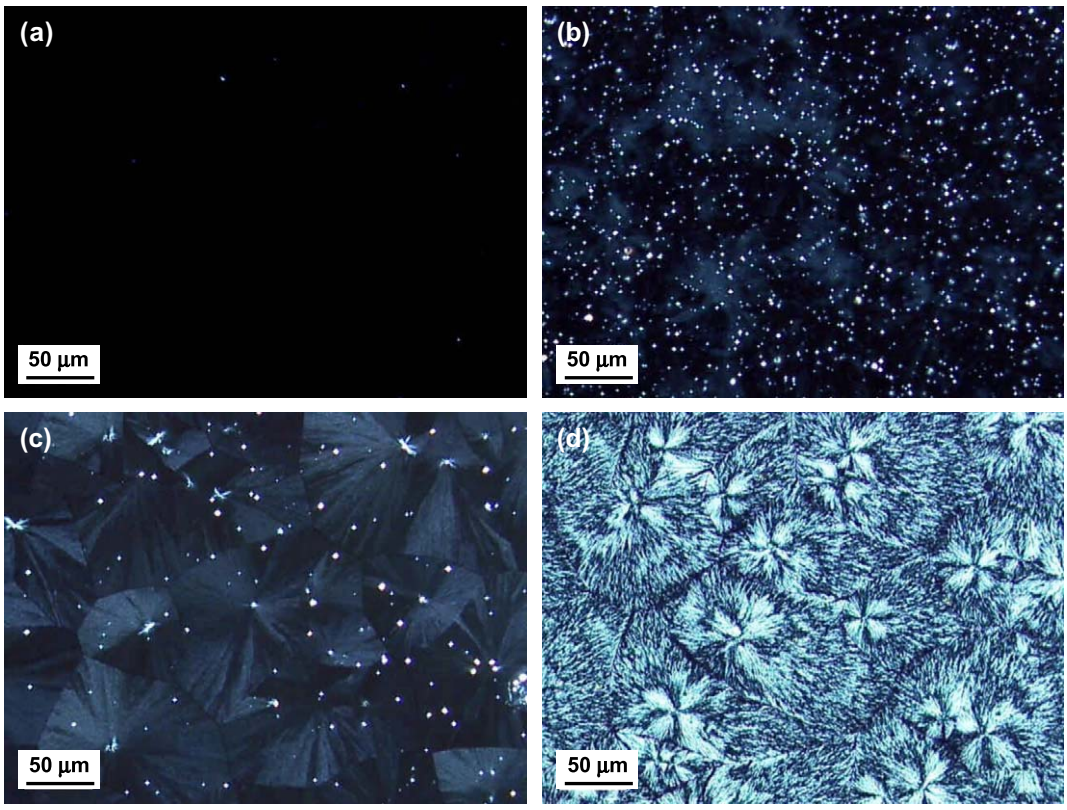

Fig. 2. Polarized optical microscopy images from freshly made nanocomposite films of different composition. The top surface of films is shown. (a) LRD60%–PEO40%-1000 kg/mol, (b) LRD40%–PEO60%-1000 kg/mol, (c) LRD15%–PEO85%-1000 kg/mol, and (d) reference pure PEO-1000 kg/mol.

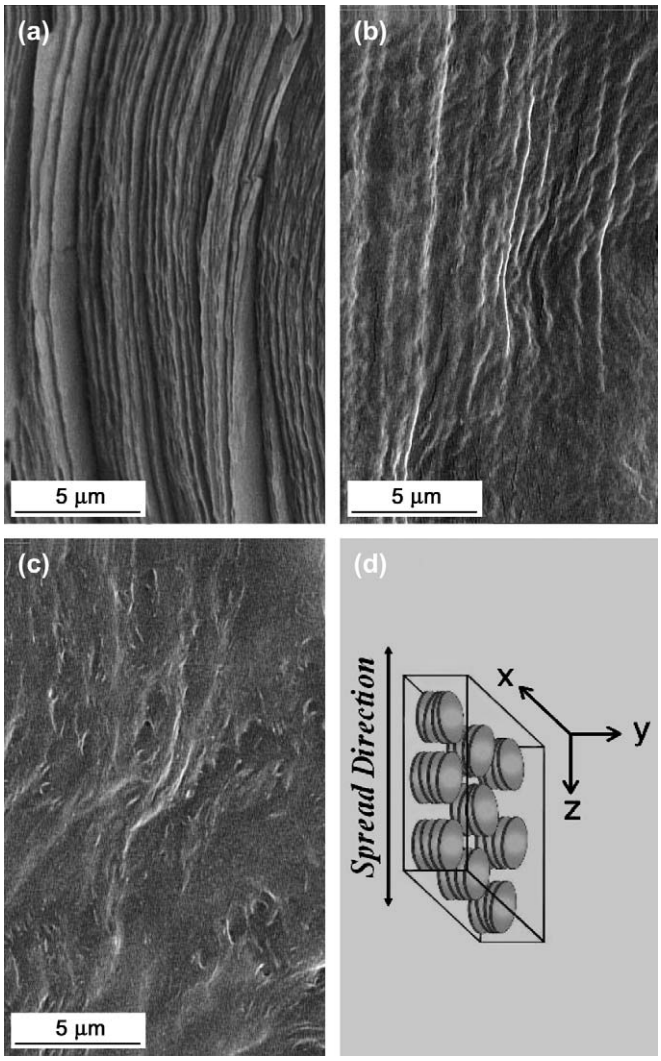

Fig. 3. SEM images from freshly made nanocomposite films of different composition. The $x-y$ plane (side surface) of films is shown. (a) LRD60%–PEO40%-1000 kg/mol, (b) LRD40%–PEO60%-1000 kg/mol, and (c) LRD15%–PEO85%-1000 kg/mol. The definition of planes is shown for better comparison of figures (d) The physical picture of general platelet orientation in the film corresponds only to (a) [11].

We have studied the micro- and nano-structures of selected LRD60%–PEO40% nanocomposite films in the past and have shown that the solution structure and processing conditions strongly influence the overall morphology of the dried films [11]. The collapse of a polymer–clay network structure as the solution dries leads to either highly oriented thick layers in the dried film (Fig. 5a) or very fine layers (Fig. 5b). The number of multilayers can only be estimated since one single spread produces multiple layers on large length scales [11]. Only representative SEM images of multilayered films in the $x-y$ planes (side surfaces) are shown in Fig. 5. On the micron length scale, the layered structures are dependent on the polymer Mw [11]. Among many other parameters, we believe that the sample preparation and the resulting structure strongly influence the crystallinity. For example, not completely exfoliated nanocomposite solutions containing pure clay aggregates will lead to films which have more excess PEO. This excess PEO is not bound to the clay and will crystallize. In the following, sample preparation and composition are kept constant to minimize defects while investigating the thermal properties of selected multilayered nanocomposite films as a function of polymer Mw.

3.2. Polymer Mw dependence of thermal properties

Fig. 6 represents the polymer Mw dependence of DSC data from (a) nanocomposite multilayered films at a constant composition of polymer and clay LRD60%–PEO40%-*X* and (b) reference pure PEO films (Table 1). All nanocomposite films have the same sample history regarding sample preparation. Comparison between our results and studies from literature are difficult due to different sample preparation techniques and sample history, which are some of the parameters that strongly influence adsorbed water content (see Section 3.3). The DSC curves shown have been normalized to the amount of 1 mg LRD60%–PEO40%-*X* and shifted for better visualization. DSC thermograms were obtained in the second heating cycle of the DSC measurement to avoid artifacts that could influence the results. This procedure removes mechanical tensions that may originate from the layering process during film formation. The same trends are observed in the first heating cycle (not shown here) but with much larger fluctuations in crystallinity between the first heating cycles compared to the second ones.

From the DSC curves shown in Fig. 6 the crystallinity of samples was calculated and included in Table 1. The melting temperature of the nanocomposites (Fig. 6a) slightly decreases with the increase in polymer Mw, the only exception from this being the sample with LRD60%–PEO40%-100. From solution studies we know that LRD60%–PEO40%-100 is the only sample where the polymer chains are too short to interconnect the clay platelets in solution [17]. This sample does not show any significant shear-orientation of platelets or stretching of polymer chains in solution. During the film spreading and drying process LRD60%–PEO40%-100 does not build the type of supramolecular structured layers as the other samples do (see Fig. 5). Since the polymer chains are not crosslinked to several platelets in solution, they do not remain elongated and stretched during the film spreading procedure. Any elongated polymer chain during shear will recoil back fast in solution. The predominant structural shear-orientation in the film that we have observed previously [18], comes from the collapse of the network structure in solution and the clay platelet orientation during solvent evaporation. The shear forces during the spreading process are not strong enough and too short to keep the polymer chains stretched. Thus these ‘‘100 kg/mol’’ long polymer chains have sufficient space and flexibility to recoil from any deformed position and crystallize. This may be one reason why LRD60%–PEO40%-100 does not follow the trend observed in Fig. 6a and why we observe a higher crystallinity for the LRD60%–PEO40%-100 than for all other samples at the same composition (Table 1).

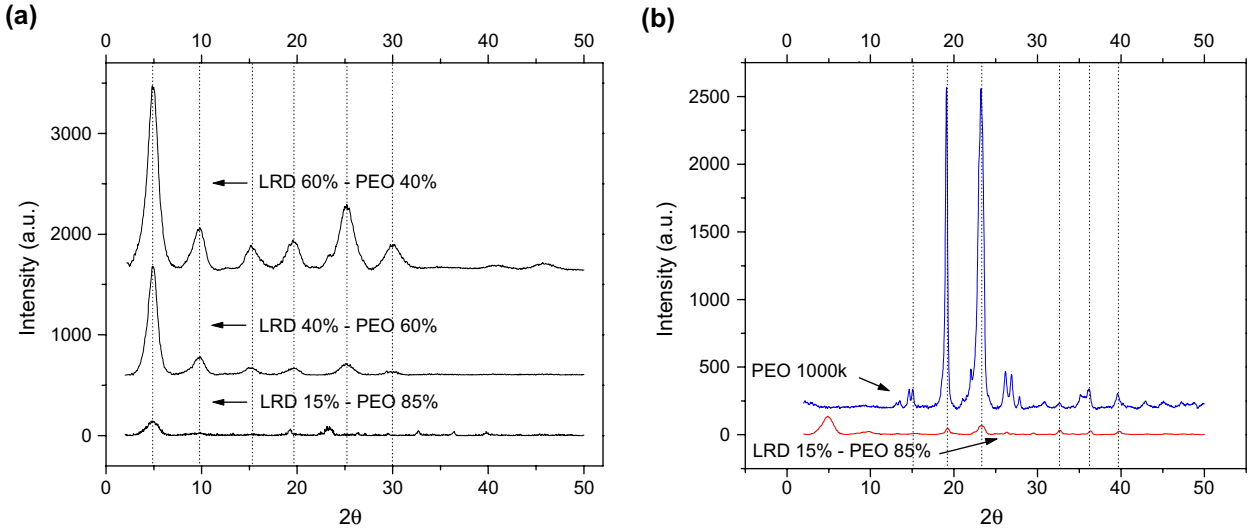

Fig. 4. (a) X-ray diffraction patterns for LRD60%–PEO40%-1000 kg/mol, LRD40%–PEO60%-1000 kg/mol, and LRD15%–PEO85%-1000 kg/mol (see also Table 1); (b) a comparison of the pure PEO-1000 kg/mol and LRD15%–PEO85%-1000 kg/mol X-ray diffraction curves.

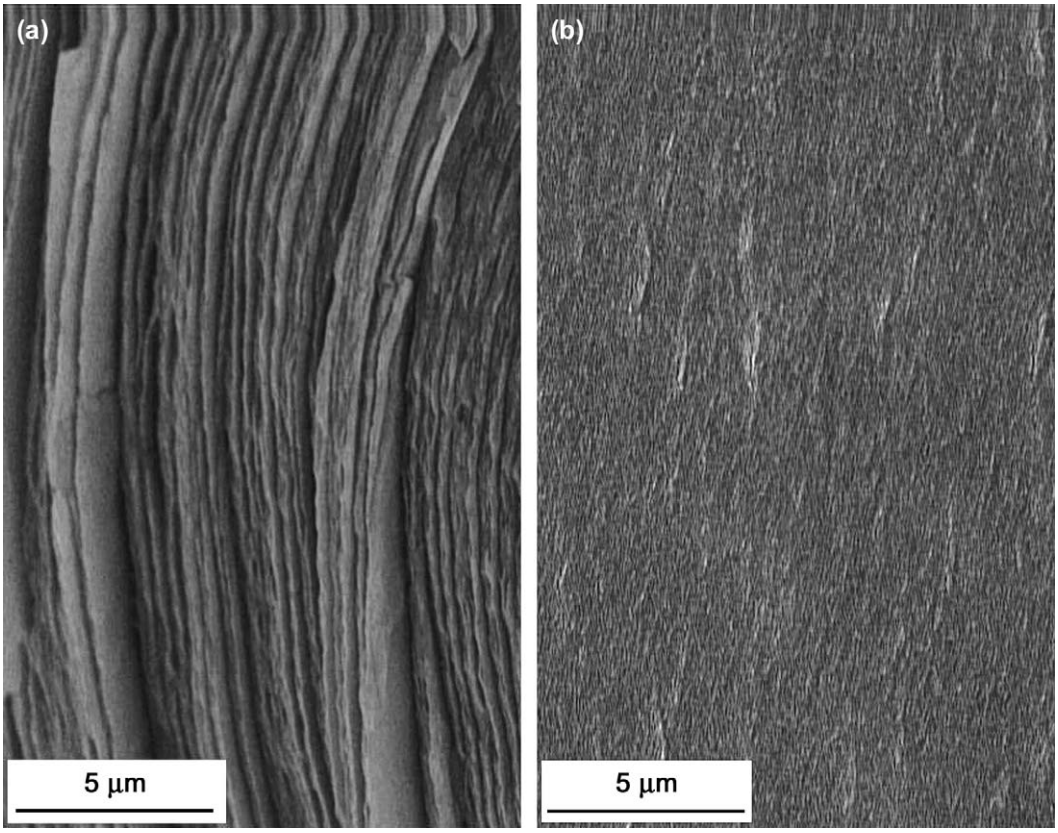

Fig. 5. SEM images from nanocomposite films of same composition but different polymer Mw. The $x-y$ planes (side surfaces) of films are shown. (a) LRD60%–PEO40%-1000 kg/mol and (b) LRD60%–PEO40%-100 kg/mol.

In the series LRD60%–PEO40%-X with $X = 300$, 600, and 1000 kg/mol crystallinity is small but increases with increasing polymer Mw and polymer chain length (linear polymers). In all these samples, polymer chains are long enough to interconnect the clay platelets in solution. During the film spreading and drying process clay platelets are oriented, polymer chains are stretched, and supramolecular structured layers are observed in all length scales [11,19,32]. Since the clay particles act as multifunctional cross-linkers, polymer chains may remain stretched during the film drying process. We do not know how many polymer chains and loops are attached to each clay platelet. These adsorbed chains and small loops will not crystallize but remain amorphous. Long polymer chains will have more interconnections with the clay particles than short

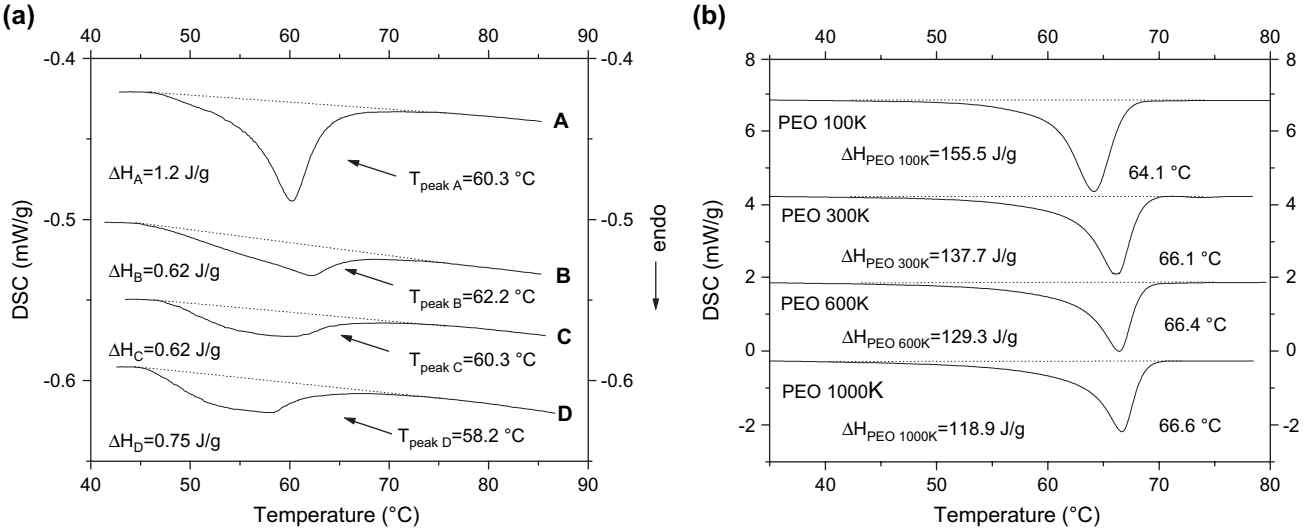

Fig. 6. Polymer Mw dependence of normalized DSC traces for the melting of: (a) LRD60%–PEO40% samples containing polymer of different molecular weights (A – 100 kg/mol, B – 300 kg/mol, C – 600 kg/mol, D – 1000 kg/mol) (see Table 1) and (b) pure PEO polymer of different molecular weights.

polymer chains whose dangling ends are not network active and cannot be stretched during shear. Dangling ends may move more easily, but they cannot phase separate during the film drying process because they are connected to the clay. Short dangling ends may recoil thus increasing the number of defects in a developing PEO crystal, while long dangling ends may crystallize. Nevertheless as shown in Fig. 6a, long polymer chains seem to better crystallize than the short chains.

Another interpretation of the results shown in Fig. 6 takes into account potential water present in the nanocomposite films. When polymer chains are adsorbed to the clay layers, water molecules initially present on the silicate surfaces and galleries are displaced to accommodate the polymer chains. This adsorption takes place in the solution as well as during the drying of the films [2]. Although the nanocomposite films have been dried in vacuum, some water molecules may still be trapped in the films. Displaced water molecules from the clay surfaces, or water molecules from the precursor solutions, are likely trapped within the PEO crystallites, shifting the melting transition to lower temperatures [2]. The calculated values for crystallinity shown in Table 1 are very similar but trends can be reproduced when measurements are repeated on ''freshly prepared'' samples. It is possible that more water molecules are present in a nanocomposite film when the polymer Mw is high, which leads to a more pronounced shifting of the melting transition to lower temperatures. In the presence of clay nanoparticles, high polymer Mw has a more disordered/amorphous structure and could accommodate more water molecules. However, since the overall differences in melting temperature are very small the amounts of incorporated water must be very small too.

Reference DSC experiments on pure PEO samples are presented in Fig. 6b. As expected we observe a decrease in polymer crystallinity with increasing polymer Mw. Crystallinity decreases, because long entangled chains have difficulties in reaching and maintaining a proper alignment necessary for crystallization. With the increase of polymer Mw, the melting temperature of the polymer slightly increases due to a higher inertia of longer chains toward movement in the melting process. Fig. 7 shows XRD from dry samples of LRD60%–PEO40%-*X*. Regular XRD reflections for all samples correspond to the PEO intercalated and stacked clay. Overall, the results suggest that there is not much polymer Mw dependence present. The first peak in XRD corresponds to a *d*-spacing of 17.8 Å, a result in agreement with what has been found in literature. Such regular reflections have been observed in the past for many other clay nanocomposites [11].

3.3. Humidity dependence of thermal properties

While the nanoparticles certainly affect the motion of the adsorbed polymer chains in the nanocomposite film, the

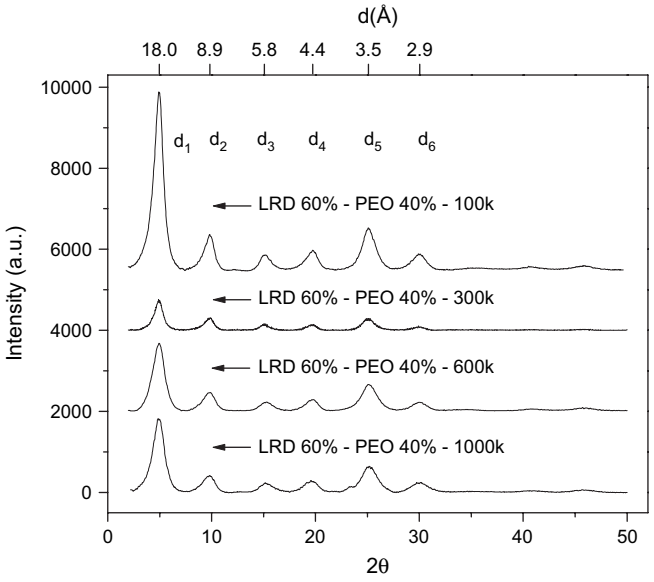

Fig. 7. X-ray diffraction patterns for LRD60%–PEO40%-*X* samples containing different Mw polymers (A – 100 kg/mol, B – 300 kg/mol, C – 600 kg/mol, D – 1000 kg/mol) (see Table 1).

presence of the water molecules and the kinetics of water adsorption strongly influence the polymer crystallinity in the multilayered films. In an effort to understand these effects better, we have examined the kinetics of water adsorption as a function of polymer Mw. Fig. 8 shows DSC curves for LRD60%–PEO40%-*X* samples exposed to humidity. The sample preparation, history and the exposure time to humidity were kept the same and duplicate measurements guaranteed reproducibility. Dry samples were exposed to humidity for 3 h, 6 h, 12 h, 24 h and 48 h. Overall, the same trends are observed for all nanocomposite films. Adsorption of water decreases crystallinity gradually until it disappears almost completely, leaving the polymer amorphous. A decrease in the polymer melting temperature can also be noticed with increased water adsorption. This may be due to smaller crystallite sizes but possibly also to the heat capacity of present water molecules surrounding the polymer. Distinguishable differences in DSC curves for the individual samples are attributed to the polymer Mw which influences the water adsorption and the kinetics of the polymer to reach a completely amorphous state. Although the LRD60%–PEO40%-1000 sample reaches an amorphous state after 12 h, we observe a small peak in the heating curve for this sample after 48 h of exposure to humidity. This trend is reproducible when the experiment is repeated. It seems like this sample has gained back some crystallinity, which may be due to internal rearrangements of the PEO chains. Upon reaching critical water content the motions of PEO chain backbones are strong enough to diffuse, twist and bend into crystallites. Surprisingly the lower polymer Mw LRD60%–PEO40%-300 sample needs 48 h of exposure to humidity to completely loose crystallinity (Fig. 8). General trends and differences between nanocomposites with different polymer Mw were also monitored with TGA (Fig. 9 and Table 2). The weight loss as function of

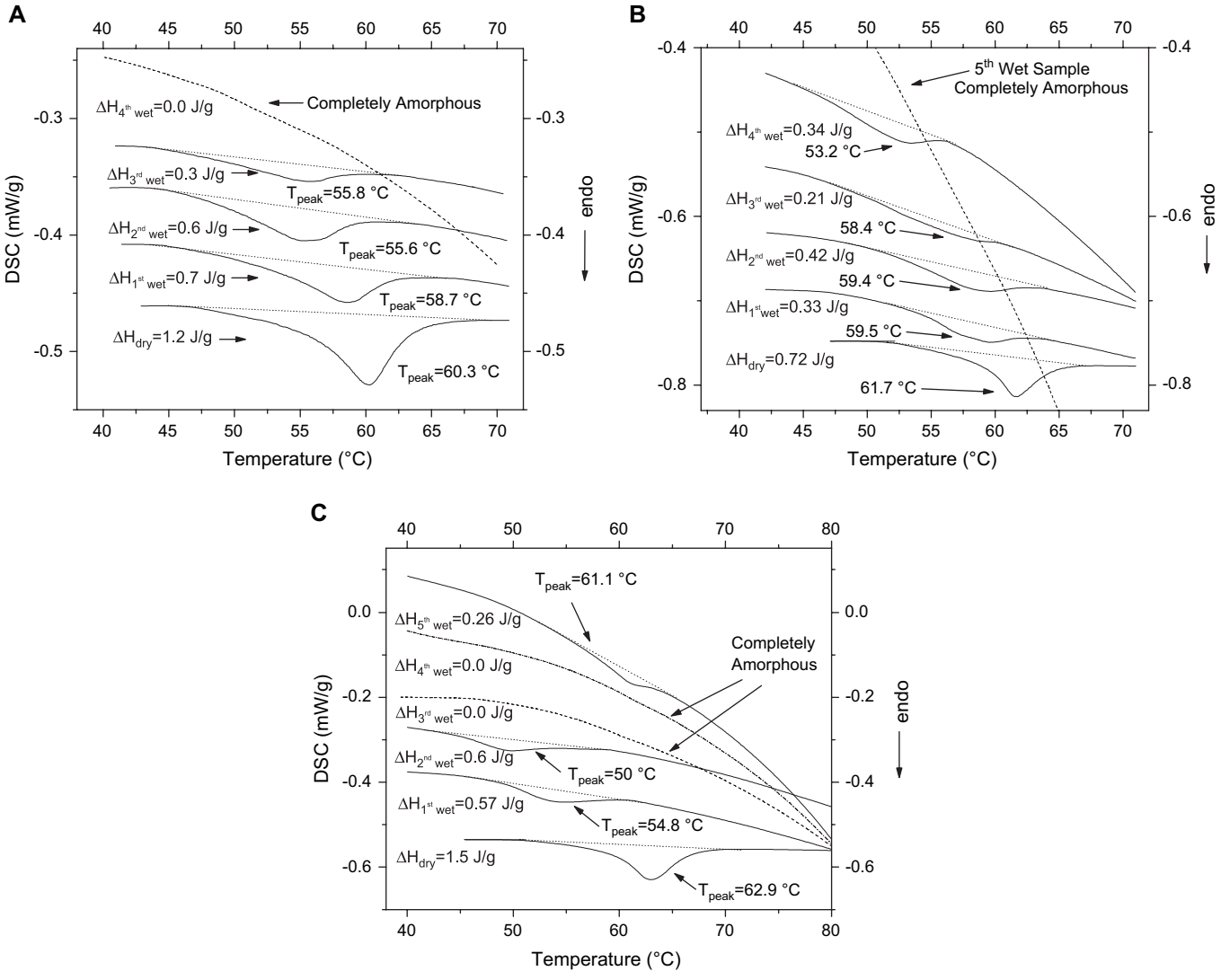

Fig. 8. Thermal analysis of nanocomposites exposed to humidity (“dry” sample – not exposed to humidity, 1st wet sample after 3 h exposure to humidity, 2nd wet sample after 6 h exposure to humidity, 3rd wet sample after 12 h exposure to humidity, 4th wet sample after 24 h exposure to humidity, 5th wet sample after 48 h exposure to humidity). (A) DSC traces for LRD60%–PEO40%-100 kg/mol, (B) DSC traces for LRD60%–PEO40%-300 kg/mol, and (C) DSC traces for LRD60%–PEO40%-1000 kg/mol.

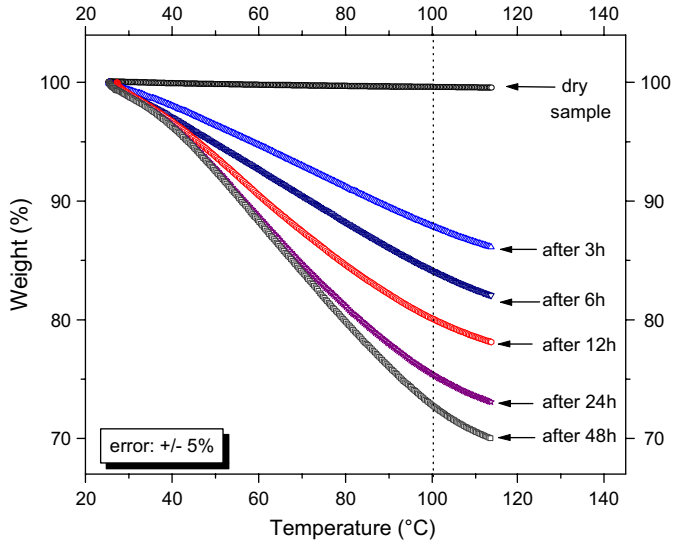

Fig. 9. Thermogravimetric analysis of LRD60%–PEO40%-1000 kg/mol exposed to humidity.

temperature shows the influence of water on the nanocomposite weight. Up to ca. 30% of water can be adsorbed in the film when measured at 100 °C. The reversible swelling of the film x–y plane as monitored by polarized optical microscopy is shown in Fig. 10. Fractured surfaces are shown for dry films and the same films are exposed to humidity. While the x–z film plane (top surface) is black under crossed polarizers (see Fig. 2a), the x–y plane is strongly birefringent due to aligned polymer and clay particles. Upon exposure to humidity a 260 μm thick film will swell up to 290 μm (Fig. 10). On a qualitative level no significant polymer Mw dependence has been observed in swelling behavior or TGA. Further experiments on many samples are necessary in order to understand the swelling behavior on a quantitative level.

Table 2
Weight loss percentage at 100 °C as resulted from the TGA measurements

Sample (exposure to humidity)	Weight loss (%), LRD60–PEO40-1000	Weight loss (%), LRD60–PEO40-300	Weight loss (%), LRD60–PEO40-100
Dry sample (no humidity)	0.39	0.37	0.34
1st wet sample (after 3 h)	12.15	13.25	10.1
2nd wet sample (after 6 h)	15.88	15.06	14.36
3rd wet sample (after 12 h)	19.94	16.98	16.68
4th wet sample (after 24 h)	24.61	19.11	22.26
5th wet sample (after 48 h)	27.23	30.05	26.2

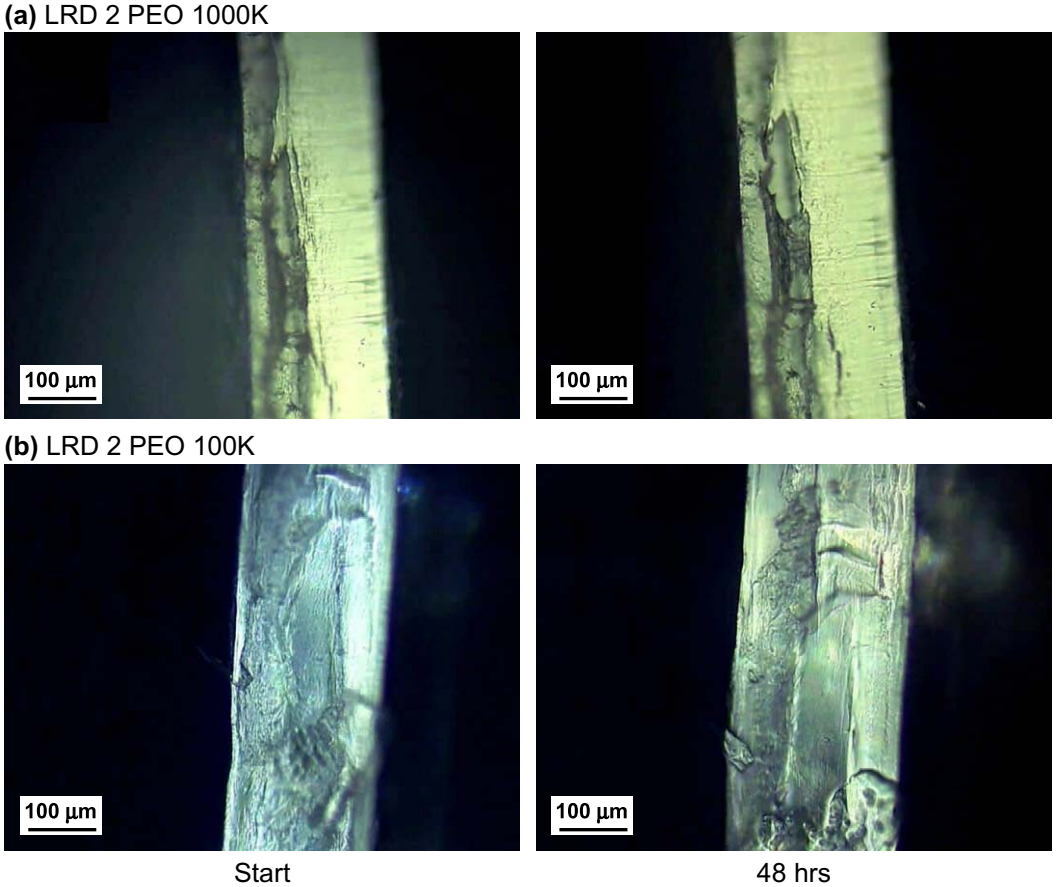

Fig. 10. Polarized optical microscopy images from nanocomposite films of same composition but different polymer Mw. The x–y planes (side surfaces) of films are shown. (a) LRD60%–PEO40%-1000 kg/mol and (b) LRD60%–PEO40%-100 kg/mol.

4. Summary

We have shown that the crystalline structure of the nanocomposite multilayered films can be tuned by controlling the composition, polymer Mw and the water content. We have studied the concentration, polymer Mw and humidity dependence on polymer crystallinity and found that sample preparation and history are important in controlling structure and properties.

Our preliminary results on the design of nanocomposite solutions and gels for film preparation are used to rapidly evaluate new and promising candidate materials for the fabrication of other hierarchical structured films. The optimization of the current film fabrication techniques will guide the preparation of transparent and multilayered films over the whole Laponite concentration range. In this work we have chosen only those solutions and gels for film preparation, where the shear rate and exact film thickness are not critical to the final film structure and where the multilayer size and order can be reproduced easily. All the other solutions and gels that have produced interesting supramolecular structures were not investigated here in detail because results could not yet be reproduced satisfactorily. In the future we will study the shear rate dependent structure formation and the relation between the relaxation after cessation of shear and the relaxation times of the polymer and the clay particles that are critical to structure formation. Future experiments will allow for characterizing the critical parameters responsible for the appearance or disappearance of polymer crystallinity. Structural studies of these materials will be then complemented by dynamic mechanical analysis.

Acknowledgment

We acknowledge financial support in part from an NSF-CAREER award, DMR 0348884. We also acknowledge the use of the Socolofsky Microscopy Center at Louisiana State University and the assistance of Cindy Henk in conducting microscopy.

References

[1] Aranda P, Mosqueda Y, Perez-Cappe E, Ruiz-Hitzky E. Journal of Polymer Science Part B: Polymer Physics 2003;41(24):3249–63.
[2] Aranda P, Ruiz-Hitzky E. Applied Clay Science 1999;15(1–2):119–35.
[3] Wu JH, Lerner MM. Chemistry of Materials 1993;5(6):835–8.
[4] Doeff MM, Reed JS. Solid State Ionics 1998;115:109–15.
[5] Sandi G, Joachin H, Kizilel R, Seifert S, Carrado KA. Chemistry of Materials 2003;15(4):838–43.
[6] Sandi G, Carrado KA, Joachin H, Lu W, Prakash J. Journal of Power Sources 2003;119:492–6.
[7] Vaia RA, Vasudevan S, Krawiec W, Scanlon LG, Giannelis EP. Advanced Materials 1995;7(2):154–6.
[8] Armand M. Advanced Materials 1990;2(6–7):278–86.
[9] Gadjourova Z, Andreev YG, Tunstall DP, Bruce PG. Nature 2001; 412(6846):520–3.
[10] Gadjourova Z, Marero DM, Andersen KH, Andreev YG, Bruce PG. Chemistry of Materials 2001;13(4):1282–5.
[11] Dundigalla A, Lin Gibson S, Ferreiro V, Malwitz MM, Schmidt G. Macromolecular Rapid Communications 2005;26(3):143–9.
[12] Chaiko DJ. Chemistry of Materials 2003;15(5):1105–10.
[13] Chaiko DJ, Leyva A, Niyogi S. Advanced Materials and Processes 2003; 161(6):44–6.
[14] Schmidt G, Nakatani AI, Butler PD, Han CC. Macromolecules 2002;35(12):4725–32.
[15] Schmidt G, Nakatani AI, Butler PD, Karim A, Han CC. Macromolecules 2000;33(20):7219–22.
[16] Schmidt G, Nakatani AI, Han CC. Rheologica Acta 2002;41(1–2): 45–54.
[17] Loizou E, Butler P, Porcar L, Schmidt G. Macromolecules 2006;39(4): 1614–9.
[18] Loizou E, Butler PD, Porcar L, Talmon Y, Kesselman E, Schmidt G. Macromolecules 2005;38:2047–9.
[19] Stefanescu EA, Dundigalla A, Ferreiro V, Loizou E, Porcar L, Negulescu I, et al. Physical Chemistry Chemical Physics 2006;8(14): 1739–46.
[20] Bujdak J, Hackett E, Giannelis EP. Chemistry of Materials 2000;12(8): 2168–74.
[21] Lagaly G. Applied Clay Science 1999;15(1–2):1–9.
[22] Lagaly G, Ziesmer S. Advances in Colloid and Interface Science 2003;100:105–28.
[23] Edman L, Ferry A, Doeff MM. Journal of Materials Research 2000; 15(9):1950–4.
[24] Strawhecker KE, Manias E. Chemistry of Materials 2003;15(4): 844–9.
[25] Ishikiriyama K, Wunderlich B. Journal of Polymer Science Part B: Polymer Physics 1997;35(12):1877–86.
[26] Ishikiriyama K, Wunderlich B. Macromolecules 1997;30(14):4126–31.
[27] Qiu WL, Pyda M, Nowak-Pyda E, Habenschuss A, Wunderlich B. Macromolecules 2005;38(20):8454–67.
[28] Aray Y, Manuel M, Rodriguez J, Vega D, Simon-Manso Y, Coll S, et al. Journal of Physical Chemistry: B 2004;108(7):2418–24.
[29] Aray Y, Marquez M, Rodriguez J, Coll S, Simon-Manso Y, Gonzalez C, et al. Journal of Physical Chemistry: B 2003;107(34):8946–52.
[30] Vogt BD, Soles CL, Lee HJ, Lin EK, Wu WL. Langmuir 2004;20(4): 1453–8.
[31] Schwarz B, Schonhoff M. Langmuir 2002;18(8):2964–6.
[32] Malwitz MM, Dundigalla A, Ferreiro V, Butler PD, Henk MC, Schmidt G. Physical Chemistry Chemical Physics 2004;6(11): 2977–82.
[33] Malwitz MM, Butler PD, Porcar L, Angelette DP, Schmidt G. Journal of Polymer Science Part B: Polymer Physics 2004;42(17): 3102–12.
[34] Malwitz MM, Lin-Gibson S, Hobbie EK, Butler PD, Schmidt G. Journal of Polymer Science Part B: Polymer Physics 2003;41(24): 3237–48.